Determination of Print Speed Based on The Fresh Mechanical Strength Over Time of Additively Constructed Concrete by Unconfined Compression

Christian Negron-McFarlane[1], Eric Kreiger[1], Megan Kreiger[1]

[1] U.S. Army Corps of Engineers, Engineer Research and Development Center, Construction Engineering Research Laboratory, United States
*megan.a.kreiger@usace.army.mil

Abstract. Additive construction is a complex process that is influenced by different factors, such as printing parameters, design and construction, as well as materials properties. Since no formwork is used, a fundamental understanding of shape stability and print stability is required to ensure the successful completion of printed components. Additionally, utilizing additive construction in remote field applications increases the variables associated with printing and requires a quantifiable methodology for both laboratory and on-site to maintain quality control. This study focuses on the use of the unconfined compression test to characterize the buildability of the fresh additively constructed concrete with 9.5 mm aggregates. Mechanical properties, such as load and elastic modulus gain, were evaluated in addition to plate buckling theory to determine the print stability of the printing process based on the two primary failure mechanisms: plastic collapse and elastic buckling. This study identifies a method of determining failure parameters to identify the layer deposition limit and print speed to decrease failure during the printing process.

Keywords: Additive Construction; 3D printing; Buildability; Unconfined Compression; Layer Deposition Rate.

1 Introduction

For the additive construction (AC) process [1], the development of material properties at very early ages (0-120 min) is critical to ensuring material performance and job site safety [2]. AC concrete should be evaluated to quantify its very early age (0-120 min) performance, including pumpability, extrudability and buildability [3]. While test methods should be defined to assess future construction efforts, the focus of this work is on buildability, as it has the most risk associated with the safe completion of structures. Insufficient buildability can be characterized by four potential failure modes [4] with primary focus on two: plastic collapse and elastic buckling [4-8]. Plastic collapse is the loss of material shape stability due to insufficient material strength. Elastic buckling is the loss of component stability due to insufficient elastic stiffness. In the development

https://doi.org/10.24355/dbbs.084-202408141311-0

of expeditionary AC, researchers at the US Army Engineer Research and Development Center observed that these failure mechanisms are not only determined by the vertical build rate and height, but also by the horizontal unbraced width and any lateral resistance due to ties or component geometry. To further understanding, this paper covers the potential impact of real-world design decisions and proposes a design process comparing material resistance against material demand during the additive construction (AC) process.

2 Background

At very early ages the material resistance is impacted by the time evolution of the material, typically described by a linear model [9] or an exponential model [10]. The evolution of compressive resistance can be determined based on direct compression results by performing measurements at increasing time intervals [7, 11, 12]. Using this testing it has been shown that the demand strength and stiffness dependent on the vertical build rate can be compared directly to the measured resistance stress and stiffness [7, 9, 11], as shown in Fig. 1. A failure of a component occurs when the material demand surpasses material resistance.

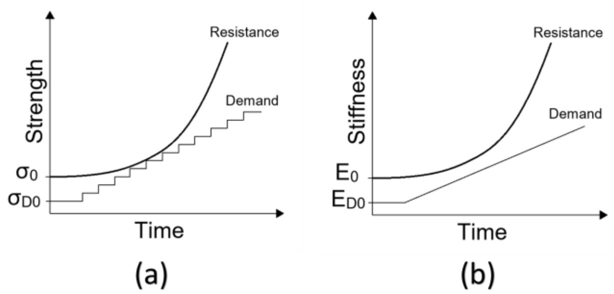

Fig. 1. (a) Stress and (b) stiffness comparative temporal plots

There are several approaches to determine buildability of additively constructed concrete including column analysis [5, 9, 10, 13] and plate theory [7, 11, 14]. Models have been developed to predict failure and define criteria for plastic collapse based on gravity loads, elastic buckling, and plate theory to accurately predict failures of thin-walled elements [7, 11, 14]. Column analysis reports show high variability in predictions and may not be appropriate for components with slender plate elements with restrained boundary conditions, such as those depicted in Fig. 2. The unbraced width of the plate can be taken to be equal to the distance between infill contact points or cross ties as depicted in Fig. 2.

https://doi.org/10.24355/dbbs.084-202408141311-0

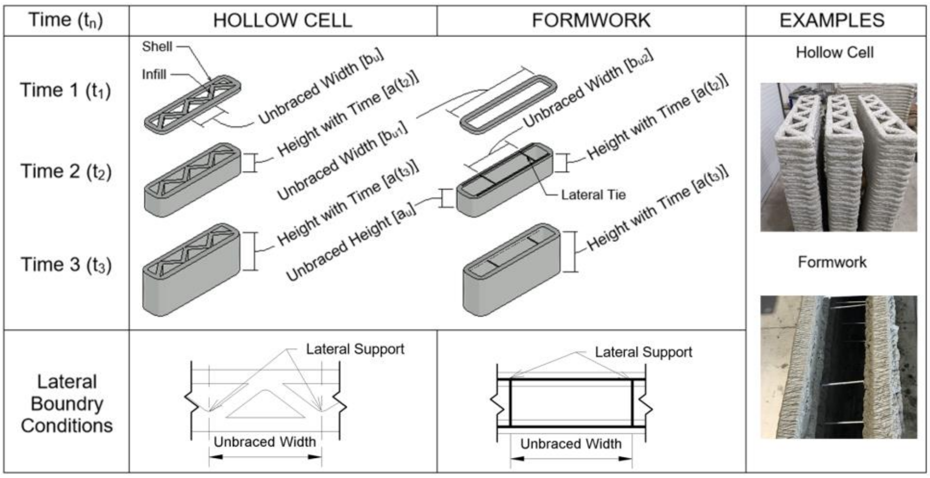

Fig. 2. Component geometry with unbraced widths and boundary conditions.

As a result of the infill-to-shell connection or wall ties, depicted in Fig. 2, there is expected to be horizontal lateral support conditions. In general, the braced shell portions of the components can be represented as plate elements with simply supported boundary conditions on all sides, depicted in Fig. 3, with a vertical compression load equal to $\rho g h$, where ρ is the density, g is the acceleration due to gravity and h is the height of the plate. Alternatively, a plate simply supported at the top and bottom in the direction of loading with free end conditions in the horizontal direction, representative of a column, can also be calculated as the more conservative case. The former condition will be referred to a simply supported and the latter will be referred to as free.

The loaded plate is defined by a thickness, *t*, width, *b*, and height, *a*, as depicted in Fig. 3a. From the equation for elastic buckling load, the critical stress can be calculated for a plate [15] with Eq. (1):

$$\sigma_{cr} = k_c \frac{\pi^2 E}{12(1-\nu^2)} \left(\frac{t}{b}\right)^2 \tag{1}$$

Where E is the elastic modulus and ν is the Poisson ratio. Coefficient k_c in the equation corresponds to the plate buckling coefficient, which is a function of the plate geometry and boundary conditions. The buckling coefficient is related to the buckling modes derived from out-of-plane displacement, $d_1(x, z)$ at buckling onset proportional to the product of sine functions in x and z directions, where n corresponds to the number of half waves in the x direction, and m corresponds to the number of half waves in the z direction, depicted in Fig. 3b. The minimum value of k_c occurs where (n = 1) for the simply supported condition and (n=0, m=1) for the free condition, respectively. To minimize the value for k_c based on the plate aspect ratio, a/b, for the simply supported condition m changes as shown in Fig. 3c. In this approach, imperfections from manufacturing tolerances are not considered, only vertical variation.

https://doi.org/10.24355/dbbs.084-202408141311-0

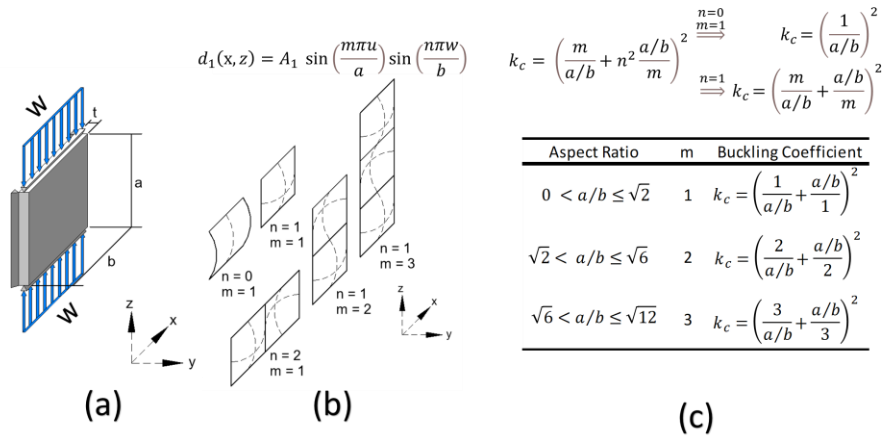

Fig. 3. (a) Simply supported plate, (b) half waves associated with buckling modes and (c) equations to calculate the buckling coefficient.

In the determination of the expected failure limit states for project specific geometries buildability (stability) testing may be necessary to confirm if and type of failure that is expected [5, 7-8]. Furthermore, during the AC of large structures quality control should be performed. This has been demonstrated through documentation of layer print times, delay times between layers, print quality, deviations from design, and environmental conditions, which can then be compared to experimental material and structural data [16-17]. Data may include lab tested strength and elastic modulus development and print stability [6] in addition to in-situ conditions [2, 12, 16]. Data then can be compared to field documented data to confirm if material deviations are expected, failure limit states are passed, or cold joints will be present [2].

The models presented in literature on plastic collapse and elastic buckling assume continuous operations to complete a single component and no additional weight due to reinforcement or wall ties [5-6]. In reality, components are produced in series, placing multiple layers on an individual component prior to moving to the next, adding complexity to failure prediction. Furthermore, most studies use mortar materials [17], which do not consider the impact of coarse aggregate [18]. It is of interest to know how the buildability differs for concrete mixtures with coarser aggregate sizes, as these materials can effectively inhibit shrinkage and creep, and lead to cost and carbon savings due to reduction binders [19-20].

In this paper, the authors propose a model that simplifies validation of structural components in the process of additive construction, with the objective to identify a suitable process to directly compare design to testing used for quality assurance and quality control. The intent is to provide engineers with a methodology to determine the print speed based on the size of the component, number of components, number of continuous layers produced per element, reinforcement placed during construction; with minimal risk of failure and complete the process in the shortest amount of time. The paper provides

https://doi.org/10.24355/dbbs.084-202408141311-0

an evaluation of the strength and stiffness evolution for concrete with a nominal maximum aggregate size of 9.5 mm using the unconfined compression test and an analysis of buildability of components made with concrete materials using a discrete time (or layer) analysis that can incorporate more complicated layer times and additional weight due to reinforcement/ties. The analysis will be based on compression for plastic collapse and plate theory for elastic buckling and builds a theoretical framework that is in agreement with practice, but may require refinement using experimental data.

3 Materials and Methods

3.1 Materials and mixing procedure

Mixture consisted of Type 1L (Portland-Limestone) cement, pea gravel with a nominal maximum aggregate size of 9.5 mm, sand, a thixotropic modifier, and a high range water-reducer. This mixture meets shape stability requirements and mixture process covered in prior research by the U.S. Army Engineer Research & Development Center [12].

3.2 Equipment and procedures

An electronic load frame was used to perform unconfined compression on a specimen of 50mm height and 75mm width with height/width of 1.5 representative of a single bead. Testing was performed during the first two hours after mixing, at intervals of 15 min through 90 min followed by 30 min intervals at times greater than 90 min. Each test age was performed in triplicate and were reported using the average of the results. Testing was performed up to 35% strain but cut-off at 25% for reporting. The displacement rate was 50 mm/min. An analysis of stress-strain results utilized a bi-linear model. More details can be found in [12].

4 Results and Discussion

To determine the design print speed, this study performed a failure analysis by comparing the time evolution of the plastic strength and elastic modulus to the applied load based on the expected self-weight of a plate and the determination of the required stiffness based on plate buckling theory.

4.1 Unconfined compression

Load-displacement and stress-strain curves are shown (Fig. 4a and 4b). As expected, the strength increases with increased age. Similar to previous studies [6-7, 12], the compressive behavior at ages of $\leq$ 90 min can be represented using a bi-linear strain hardening model, where the linear strength increases until an elastic limit, at which the rate of

https://doi.org/10.24355/dbbs.084-202408141311-0

strength gain decreases until a plastic limit. At 120 min the material exhibits strain hardening up to a peak followed by strain softening. Although it is not shown, the samples behave as an integral body with plastic deformation rather than failing by shear on distinct plane due to the compactness of the specimens.

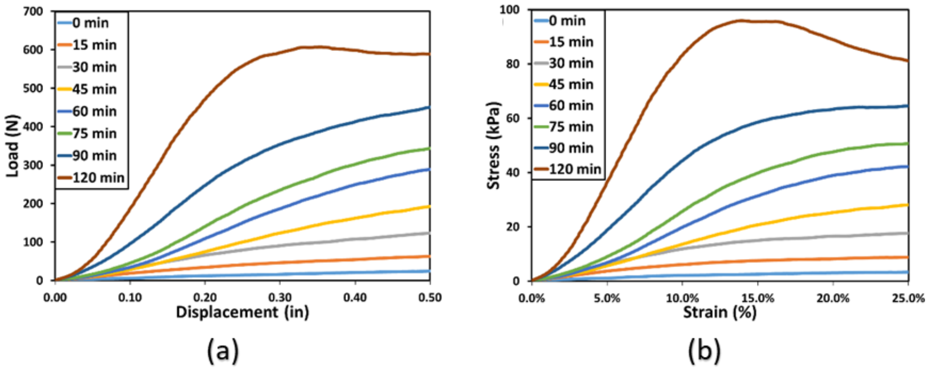

Fig. 4. Load-displacement (a) & stress-strain (b) in compression tests for concrete age 0-120 min.

Based on a previous study [12] the elastic limit and the plastic limit were determined to be at 7.5% and 18.7%, respectively. 7.5% strain provides a practical limit in the printing process since significant deformations would compromise the geometrical accuracy of the object. 18.7% strain aligns well with surface crack formation. For simplicity these values were used for ages up to 90 min. The plastic limit for the 120 min results were associated with strain at the maximum strength. For this study only the elastic modulus and the plastic stress of the material are of concern. Fig. 5 depicts the material evolution for these properties with the associated equations.

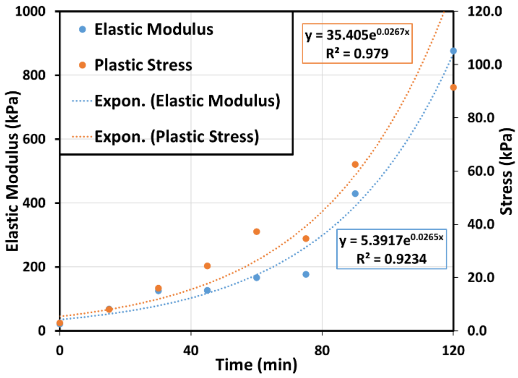

Fig. 5. Young's modulus & plastic stress from unconfined compressive of concrete specimens.

https://doi.org/10.24355/dbbs.084-202408141311-0

4.2 Design and Print Speed

The design of components can be done by the prediction of failure modes (i.e., plastic collapse and elastic buckling) against the material resistance collected from experimental data. This allows engineers to select the best design option to maximize speed of construction, in-service structural performance, and lowers risk of construction failures. Currently, it is not uncommon for printer operators to use rules of thumb (ex. 3 min/layer), which may be based on experience with one material and not reliant on data or an analysis. It is therefore critical that realistic analyses be produced that have been validated by experimental data. The following example describes a proposed process an engineer may use to determine the speed of the nozzle and vertical build rate, which is representative of real world experience, but still needs experimentally validated.

Selection of Print Speed – Example. In the design of walls with a geometry, such as, the hollow cell (Fig. 6a) or the formwork walls (Fig. 6b) with parameters indicated by Fig. 2, a designer may look at the maximum unbraced width, minimum layer times, type of lateral support, and horizonal reinforcement placement. This example will look at these criteria for the construction of four walls similar to those in Fig. 6c that are 1.2 m long, 0.91m tall, and 0.23 m wide with design parameters summarized in Table 1.

(a) (b) (c)

Fig. 6. Wall geometry: (a) hollow cell and (b) formwork with lateral ties and interior reinforcement.

Table 1. Printing and material parameters of the process

Parameters	Notation	Value
Bead thickness	t_b	0.051 [m]; 2 [in]
Wall total height	a_t	0.914 [m]; 36 [in]
Layer height	a_i	0.025 [m]; 1 [in]
Wall thickness	-	0.203 [m]; 8 [in]
Unbraced width	b	20, 40, 60, 80 [cm]; 8, 16, 24, 32 [in]
Layer time	T_l	0.5, 1 & 2 [min / layer]
Concrete Density	ρ	2159 [kg/m^3]
Poisson ratio	ν	0.892
#4 reinf. bar mass	w_s	1 kg/m

With the design of smaller components, such as these walls, the designer should look at the speed of placement and number of items produced. If too few items are produced a failure may occur. However, if too many items are produced cold joints may occur at each layer, similar to larger construction projects with long layer times. A designer may start by evaluating a single unbraced width at different layer times, followed by the unbraced width, and then the placement of reinforcement. The experimental data (i.e. material resistance) in the following figures is obtained from Fig. 5. Elastic modulus and strength demands were calculated for a continuous and a time adjusted process of 4 components on increments of 2 layers of each wall deposited in sequence with a layer time, time to start the next layer for a single wall, of 0.5, 1, and 2 minutes. For the single wall the time gap is equal to the layer time. For the time adjusted process the maximum time gap is 3.5, 7, and 14 minutes for 0.5, 1, and 2 minutes per layer, respectively.

For simplicity this approach assumes the elastic modulus of the entire plate evolves equally with the first layer, which is not representative of the actual case where each layer will have a different elastic modulus. To incorporate such behavior a modification to the model may be required based on experimental data.

A comparison of the weight added and the estimated elastic modulus demand based to the evolution of the critical stress and elastic modulus is depicted in Fig. 7 and 8, respectively. The solid and dotted lines in Fig. 7 and 8 represent the continuous and adjusted print process, respectively. The elastic modulus evolution is based on the increase in wall height per layer and an unbraced width of 0.2 m. Fig 7 shows the comparison between the calculated elastic modulus from the plate buckling equation and the elastic modulus of the material. Fig 7a considers a continuous printing process with two boundary conditions, free and simply supported (SS). Regardless of the layer time elastic buckling occurs on segments with free support conditions. For simply supported, there is no failure. Fig 7b considers an adjusted print process as previously mentioned. For free support conditions failure occurs for 0.5 min and 1 min per layer. Similar to Fig 7a there is no failure for the simply supported condition.

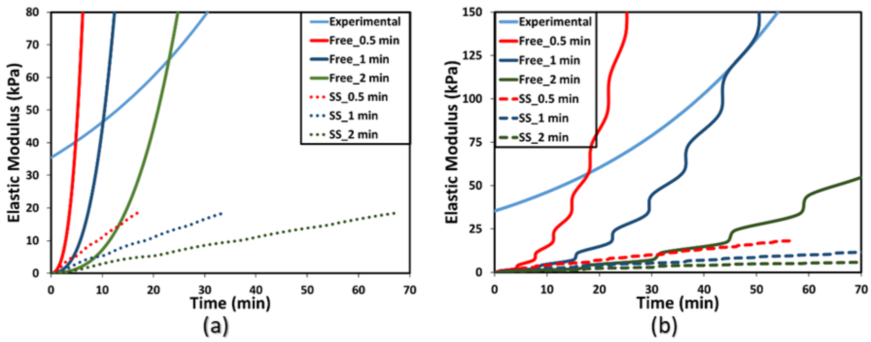

Fig. 1. Elastic modulus of single component (a) and adjusted layer design (b) and experimental approaches over time for different time per layer speeds considering different boundary conditions

Fig 8a and b shows the critical stress for a continuous and adjusted process considering both support conditions. For a continuous process as depicted in Fig 8a there is a failure occurring for 0.5 and 1 min speeds. It is worth mentioning that critical stress is the same

https://doi.org/10.24355/dbbs.084-202408141311-0

for both support conditions for each layer time. In Fig. 8a, the faster layer times of 0.5 and 1 min per layer speeds results in the strength demand exceeding the resistance for a single wall. This will result in plastic collapse failure. Whereas the 2 min layer time for a single wall results in the strength resistance exceeding the demand. Similar to Fig 8a, critical stress is the same for both conditions for a specific speed as depicted in Fig 8b. Due to the adjustments, there is no plastic collapse for the speeds studied.

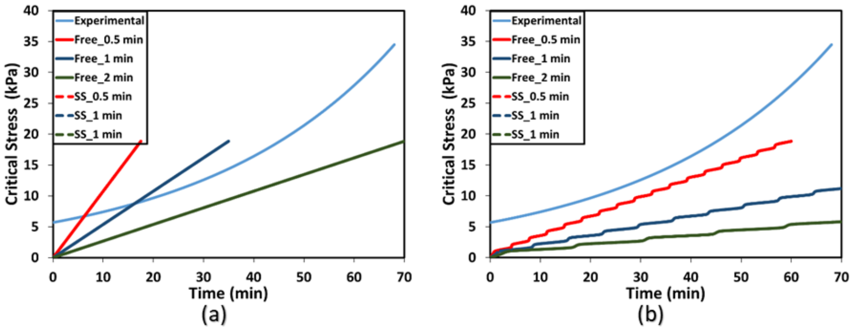

Fig. 8. Critical stress for single (a) and adjusted layer design (b) and experimental approaches over time for different time per layer speeds considering different boundary conditions.

Based on these plots the adjustment process provides more time for the material to gain strength and stiffness thus reducing the risk of failure compared to the continuous process. Another observation is that a layer time of 2 min resulted in the safest time for both free and simply supported conditions. Provided, that the typical layer time is similar for walls depicted in Fig. 6c no failure is expected. As a result and based on previous experience, a speed of 1 min per layer is selected and an adjusted print process is chosen.

The stiffness resistance curve to the demand elastic modulus gains for unbraced widths of 20, 40, 60, and 80 cm at 1 min layer times for an adjusted process considering both support conditions is depicted in Fig 9. The plot for free end condition does not change with unbraced width. However, as the unbraced width for a simply supported segment increases the risk of failure increases and the curve approaches the free end condition. This inverse relationship with unbraced length and time to failure is characteristic to what has been observed by the authors in the lab/field. From this plot the unbraced widths of 20, 30, 40 and 60 cm are not expected to result in elastic buckling.

https://doi.org/10.24355/dbbs.084-202408141311-0

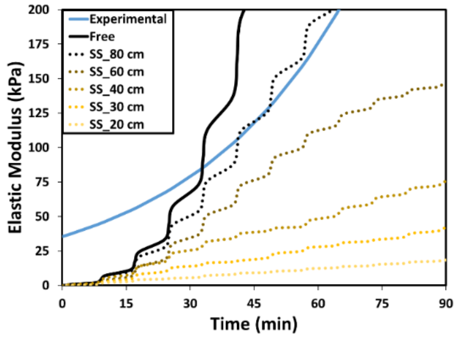

Fig. 9. Elastic modulus for different unbraced widths for the adjusted process,1 minute per layer.

Where horizontal reinforcement is needed between layers, the additional weight may result in a structural failure during construction. Fig. 10 compares the resistance curves to the demand for critical stress (Fig 10a) and elastic modulus (Fig. 10b) where #4 (12.7 mm diameter) bars are under four different reinforcement schedules. Scenario I has no reinforcement, scenario II and III involves 1 bar every 2 layers & 6 layers, respectively. Lastly, scenario IV includes 2 bars every 2 layers; all of them are done for walls with an unbraced length of 60 cm, which resulted in no failure (refer to Fig 9).

Scenario IV results in elastic buckling, which is associated with reinforcement supported by ladder wire or ties in the interior of a shell wall with cross ties spaced at 60 cm (Ex. Fig. 6c). Besides scenario IV, the elastic modulus while increasing as more reinforcement is added does not show a failure. Same occurs for Fig 10b where there is no plastic collapse for any of the scenarios. It is understandable to infer that no failure will occur with unbraced lengths lower than 60 cm. If a single wall were produced or a layer time of 0.5 min was used a collapse would be likely. This highlights the importance of accounting for the weight of reinforcement in the construction process.

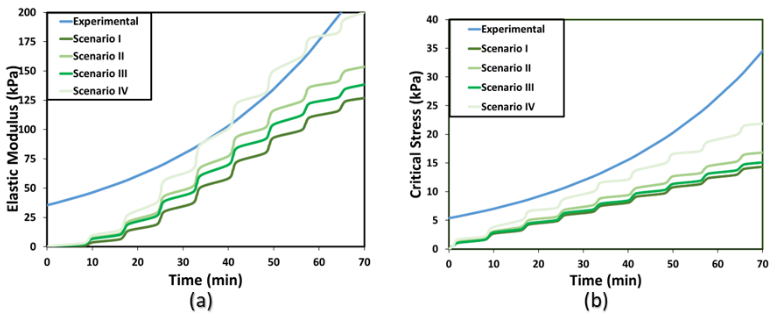

Figure 10. Elastic modulus (a) and critical stress (b) of the adjusted layer design with reinforcement and experimental approaches over time for different time for simply supported specimens.

https://doi.org/10.24355/dbbs.084-202408141311-0

Based on results a total of 4 1.2 m long x 0.91 m tall x 0.23 m wide walls with a layer time of 1.0 min, including travel between walls, can have an unbraced width of 60 cm or below. The horizontal reinforcement can be as dense as 1 #4 in placed at a minimum vertical spacing of 51 mm. With the maximum total path length, assuming an 20 cm unbraced length, for a single wall being 66 cm the maximum horizontal nozzle speed is 66 cm/min. The material deposition process consists of lifts consisting of 2 sequential layers being deposited for each wall during a single lift. For a 1 minute layer time this results in a lift time of 8 minutes resulting in a vertical build rate of 25.5 mm/min with a lift time gap of 6 minutes and a layer time gap of 7 minutes.

5 Conclusions

In practice the use of highly conservative design methods, such as column analysis of walls using AC, may result in uneconomical or inefficient designs. Furthermore, highly complex analysis methods may not be practical for field checks in expeditionary applications. This paper presents a model framework and a simplistic design approach that uses the unconfined compression data over time to characterize additively constructed concrete buildability using a time analysis incorporating the applied weight and plate buckling theory. This enables the engineer to design components based off and compared with experimental data which can be obtained from the unconfined compression testing over time. Alternating between components enables the material more time to gain stiffness and strength thus lowering the risk of failure. Reinforcement placement needs designed for in the fresh state when placing reinforcement directly on the fresh printed object, as not doing so can result in failure. Given that the predictions of the safe layer times for four 1.2 m long x 0.91 m tall x 0.23 m wide wall samples and the inverse dependency on unbraced width with time/height of the model that have been observed by the authors, further study is recommended. An experimental framework needs to be performed to test different iterations to validate and prove the significance of this prediction model.

References

1. ISO/ASTM 52939:2023 - Additive manufacturing for construction — Qualification principles — Structural and infrastructure elements (2023) www.iso.org/standard/81177.html
2. Diggs-McGee, B. and Kreiger, E., 2021, December. Using Isolated Temporal Analysis to Aid in the Assessment of Structural Element Quality for Additive Construction. In Symposium on Standards Development for Cement and Concrete for Use in Additive Construction (pp. 117-143). ASTM International
3. Le, T.T., et.al, 2012. Mix design and fresh properties for high-performance printing concrete. *Materials and structures*, *45*, pp.1221-1232.
4. Khan, S.A. and Koç, M., 2023. Buildability analysis of 3D concrete printing process: a parametric study using design of experiment approach. *Processes*, *11*(3), p.782.

https://doi.org/10.24355/dbbs.084-202408141311-0

5. Tripathi, A., Nair, S.A. and Neithalath, N., 2022. A comprehensive analysis of buildability of 3D-printed concrete and the use of bi-linear stress-strain criterion-based failure curves towards their prediction. *Cement and Concrete Composites*, *128*, p.104424.Lyu, Fuyan, et al. "Overview of the development of 3D-Printing concrete: A review." *Applied Sciences* 11.21 (2021): 9822.
6. Suiker, A.S.J., 2018. Mechanical performance of wall structures in 3D printing processes: Theory, design tools and experiments. International Journal of Mechanical Sciences, 137, pp.145-170.
7. Wolfs, R.J.M. and Suiker, A.S.J., 2019. Structural failure during extrusion-based 3D printing processes. The International Journal of Advanced Manufacturing Technology, 104, pp.565-584.
8. Suiker, A.S., et. al, 2020. Elastic buckling and plastic collapse during 3D concrete printing. *Cement and Concrete Research*, *135*, p.106016.
9. Roussel, N., 2018. Rheological requirements for printable concretes. *Cement and Concrete Research*, *112*, pp.76-85.
10. Perrot, A., Rangeard, D. and Pierre, A., 2016. Structural built-up of cement-based materials used for 3D-printing extrusion techniques. *Materials and Structures*, *49*, pp.1213-1220.
11. Wolfs, R. J. M., Bos, F. P., and Salet, T. A. M. "Early age mechanical behavior of 3D printed concrete: Numerical modelling and experimental testing," *Cement and Concrete Research*, V. 106, 2018, pp. 103–16.10.
12. Negrón-McFarlane, C., et.al, 2023. Development of In-Place Test Methods for Evaluating Printable Concretes. *Materials Journal*.
13. Weng, Y., et.al, 2018. Design 3D printing cementitious materials via Fuller Thompson theory and Marson-Percy model. *Construction and Building Materials*, *163*, pp.600-610.
14. Suiker, A.S., et. al, 2020. Elastic buckling and plastic collapse during 3D concrete printing. *Cement and Concrete Research*, *135*, p.106016.
15. Rees, David W. A., Mechanics of Optimal Structural Design: Minimum Weight Structures, John Wiley & Sons, Ltd, 9 October 2009, ISBN:9780470746233 |Online ISBN:9780470749784 |DOI:10.1002/9780470749784
16. Kreiger, E., Diggs-McGee, B., Wood, T., et al. "Field Considerations for Deploying Additive Construction." RILEM Bookseries, vol. 28. Springer, 2020. pp. 1147–63.
17. Buswell, R.A., et.al, 2018. 3D printing using concrete extrusion: A roadmap for research. *Cement and Concrete Research*, *112*, pp.37-49.
18. Sasikumar, A., et. al, 2023. Effect of coarse aggregate content on the rheological and buildability properties of 3D printable concrete. *Construction and Building Materials*, *392*, p.131859.
19. Vespalec, A., Podroužek, J. and Koutný, D., 2023. DoE Approach to Setting Input Parameters for Digital 3D Printing of Concrete for Coarse Aggregates up to 8 mm. *Materials*, *16*(9), p.3418.
20. Wang, X., et. al, 2022. Optimization of 3D printing concrete with coarse aggregate via proper mix design and printing process. *Journal of Building Engineering*, *56*, p.104745.

https://doi.org/10.24355/dbbs.084-202408141311-0